CHIN. PHYS. LETT. Vol. 38, No. 4 (2021) 045204

Coriolis Force Effect on Suppression of Neo-Classical Tearing Mode Triggered Explosive Burst in Reversed Magnetic Shear Tokamak Plasmas

Tong Liu(刘桐), Lai Wei(魏来), Feng Wang(王丰)*, and Zheng-Xiong Wang(王正汹)

Key Laboratory of materials Modification by Beams of the Ministry of Education, School of Physics, Dalian University of Technology, Dalian 116024, China

(Received 14 November 2020; accepted 10 February 2021; published online 6 April 2021)

We numerically investigate the Coriolis force effect on the suppression of an explosive burst, triggered by the neo-classical tearing mode, in reversed magnetic shear configuration tokamak plasmas, using a reduced magneto-hydrodynamic model, including bootstrap current. Previous works have shown that applying differential poloidal rotation, with rotation shear located near the outer rational surface, is an effective way to suppress an explosive burst. In comparison with cases where there is no Coriolis force, the amplitude of differential poloidal rotation required to effectively suppress the explosive burst is clearly reduced once the effect of Coriolis force is taken into consideration. Moreover, the effective radial region of the rotation shear location is broadened in cases where the Coriolis force effect is present. Applying rotation with shear located between the radial positions of $q_{\min}$ and the outer rational surface always serves to effectively suppress explosive bursts, which we anticipate will reduce operational difficulties in controlling explosive bursts, and will consequently prevent plasma disruption in tokamak experiments.

DOI: 10.1088/0256-307X/38/4/045204

The neo-classical tearing mode (NTM) is one of the most dangerous macroscale magnetohydrodynamic (MHD) instabilities, and has therefore been the focus of a great deal of research in the field of fusion plasmas.[1−4] Even if classical TM is linearly stable, NTM can still be nonlinearly triggered by sufficiently large seed islands. Seed islands can originate from various magnetic perturbations, such as error fields.[5,6] NTM is able to globally deform the equilibrium magnetic topology, thereby causing significant damage in terms of the confinement of particles and energy in tokamak experiments, and may even lead to major plasma disruptions. The reversed magnetic shear (RMS) configuration is generally considered to be an advanced operating scenario, whereby a long-pulse steady-state performance can be achieved in tokamak plasmas due to the favorable confinement properties of RMS.[7−10] During RMS discharges, an internal transport barrier (ITB) can be triggered, so that a high plasma pressure can be maintained in the core region. As such, the RMS configuration has been proposed as a prime candidate for use in the operation of future large-scale tokamak devices, such as ITER. Despite the aforementioned advantages of RMS, pairs of rational surfaces with same helicities can occur in the RMS configuration, due to the non-monotonic safety factor q-profile, which allows perturbations on each surface to couple with its counterpart, leading to the development of a dangerous MHD instability, known as the double tearing mode (DTM).[11−15] The fast reconnection of the magnetic field line caused by DTM results in the off-axis sawtooth phenomenon, and a consequent rapid collapse of plasma pressure in the core plasma region.[16−20] In order to avoid this pressure collapse and control DTM, extensive efforts have been devoted to the investigation of different kinds of techniques, such as electron cyclotron current drive,[21] externally applied toroidal shear flow,[22] resonant magnetic perturbation,[23,24] and three-dimensional MHD spectroscopy.[25] Moreover, spontaneously excited poloidal rotation via the Hall effect also significantly modifies the dynamic behaviors of DTM.[26]

With the aim of analyzing resistive MHD activities during JT-60 tokamak RMS discharges, Ishii *et al.* numerically investigated the nonlinear evolution of the DTM for a group of q-profiles, with different separations $\Delta r_{\rm s}$ between the two rational surfaces.[27,28] They noted the occurrence of an explosive burst of the DTM's perturbed kinetic energy after the Rutherford phase in the intermediate $\Delta r_{\rm s}$ case, which is considered to be a possible cause of the disruptive termination observed in the JT-60 RMS experiments. Based on Ishii's results, the effect of neo-classical current was further considered in the study reported by Wang *et al.*[29] Their numerical simulation results show that, even in the case of large $\Delta r_{\rm s}$, an explosive burst can still be triggered, given a sufficiently large fraction of

Supported by the National Natural Science Foundation of China (Grant Nos. 11925501, 11875099, and 11575158), the Liaoning Revitalization Talents Program (Grant No. XLYC1802009), and the China Scholarship Council (Grant No. 201806060036).
*Corresponding author. Email: fengwang@dlut.edu.cn
© 2021 Chinese Physical Society and IOP Publishing Ltd

bootstrap current. For the purpose of suppressing this NTM triggered explosive burst, Wang *et al.* included a differential poloidal rotation into the nonlinear simulation, thereby proving the feasibility and validity of this method.[30] In their work, rotation is shown to provide a good suppressing effect only when the shear layer of the rotation profile is located near the outer rational surface. However, the effect of Coriolis force, which has demonstrated effective suppression capabilities in relation to TMs, as reported in a previous work on the subject of toroidal plasma rotations,[31,32] has not been included in Wang's simulation. Therefore, in this work, the effect of Coriolis force on the suppression of an NTM-triggered explosive burst is investigated, using MHD@Dalian Code (MD Code).[33,34] We find that Coriolis force plays an important part in the process of burst suppression. In comparison with cases without Coriolis force, the amplitude of differential poloidal rotation to prevent the occurrence of an explosive burst is clearly reduced in cases where the effect of Coriolis force is included. Moreover, a wider range, in terms of the shear layer's radial position, proves feasible as a means of effectively suppressing NTM-triggered explosive bursts.

In this work, a set of reduced MHD equations in cylindrical geometry (r, θ, z) is applied to simulate the nonlinear evolution of NTM in the RMS configuration. The normalized equations can be written as

$$\frac{\partial \psi}{\partial t} = [\psi, \phi] - \partial_z \phi - S_{\rm A}^{-1}(j - j_{\rm b}) + E_{z0}, \tag{1}$$

$$\frac{\partial u}{\partial t} = [u, \phi] + [j, \psi] + \partial_z j - \frac{2}{r}\partial_{\rm r}\omega_{\theta 0}\partial_{\rm r}\phi + R^{-1}\nabla_\perp^2 u, \tag{2}$$

$$\frac{\partial p}{\partial t} = [p, \phi] + \chi_\parallel \nabla_\parallel^2 p + \chi_\perp \nabla_\perp^2 p + S_0, \tag{3}$$

where ψ and ϕ represent magnetic flux and stream function, respectively; $j = -\nabla_\perp^2 \psi$ and $u = \nabla_\perp^2 \phi$ denote the plasma current density and vorticity along the axial direction, respectively; $j_{\rm b} = -f\frac{\sqrt{\epsilon}}{B_\theta}\frac{\partial p}{\partial r}$ denotes bootstrap current density with $f(r, \beta) = \int_0^a j_{\rm b0} r dr / \int_0^a j_{z0} r dr$ being a function of radius r and plasma β, measuring the strength of the bootstrap current fraction, $\epsilon = a/R_0$ is the inverse aspect-ratio, and B_θ is the poloidal magnetic field. The effect of Coriolis force is represented by the term $-\frac{2}{r}\partial_{\rm r}\omega_{\theta 0}\partial_{\rm r}\phi$ in Eq. (2). This term can be obtained by exerting mathematical operation $\hat{z} \cdot \nabla \times$ on the Coriolis force, $-2\omega_{\theta 0}\hat{z} \times (\nabla\phi \times \hat{z})$. The radial coordinate, r, is normalized by the plasma's minor radius. Time t and velocity V are measured in units of Alfvén time, $\tau_{\rm A} = \sqrt{\mu_0 \rho} a / B_0$, and Alfvén velocity, $V_{\rm A} = B_0/\sqrt{\mu_0 \rho}$, respectively. $S_{\rm A} = \tau_\eta / \tau_{\rm A}$ and $R = \tau_\nu / \tau_{\rm A}$ are the magnetic Reynolds number and Reynolds number, respectively, where $\tau_\eta = a^2 \mu_0 / \eta$ and $\tau_\nu = a^2/\nu$ respectively refer to the resistive diffusion time and viscosity diffusion time; $\chi_\parallel$ and $\chi_\perp$ denote the parallel and perpendicular transport coefficients, respectively, which are normalized by $a^2/\tau_{\rm A}$. The source terms, $E_{z0} = S_{\rm A}^{-1}(j_0 - j_{\rm b0})$, and $S_0 = -\chi_\perp \nabla_\perp^2 p_0$ in Eqs. (1) and (3) are chosen to balance the diffusion of the initial profiles of ohmic current and pressure, respectively. The Poisson bracket is defined as $[f, g] = \hat{z} \cdot \nabla f \times \nabla g$.

Each variable, $f(r, \theta, z, t)$, in Eqs. (1)–(3) can be written in the form $f = f_0 + \tilde{f}(r, \theta, z, t)$, with f_0 and $\tilde{f}$ being the time-independent initial profile, and the time-dependent perturbation, respectively. By applying periodic boundary conditions in the poloidal and axial directions, the perturbed fields can be Fourier-transformed as

$$\tilde{f}(r, \theta, z, t) = \frac{1}{2}\sum_{m,n} \tilde{f}_{m,n}(r, t) \exp(im\theta - inz/R_0) + c.c. \tag{4}$$

with R_0 being the major radius of the tokamak. Given the initial profiles, Eqs. (1)–(3) can be solved using the initial value code, i.e., MD code (MHD@Dalian Code). The two-step predictor-corrector method, the finite difference method, and the pseudo-spectral method are applied in the time advancement, radial, and angular directions, respectively. An ideally conducting wall is assumed as the boundary condition in the radial direction. Here, the MD code has been repeatedly benchmarked using the codes employed in Refs. [35,36].

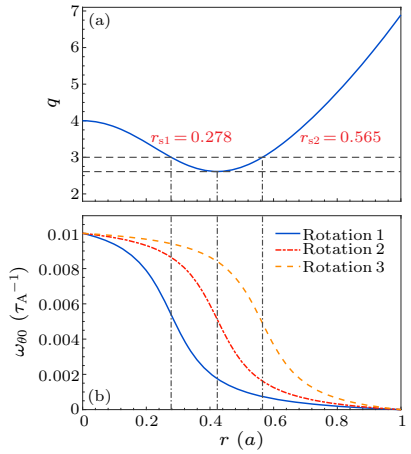

Fig. 1. (a) Initial non-monotonic safety-factor q-profile. (b) Initial rotation profiles with shear around the inner rational surface, radial position $q_{\rm min}$, and outer rational surface.

During RMS discharges in advanced tokamaks such as JT-60U, the minimum safety factor, $q_{\rm min}$, is often above 2. When optimizing both current and pressure profiles, a large pressure gradient usually exists near the ITB. Moreover, burst-like disruptions are often observed in connection with MHD activities around the $q = 3$ rational surfaces in JT-60U. Therefore, we conduct nonlinear simulations with a single helicity ($h = m/n = 3$, $0 \le m \le 36$). The q-profile adopted in this work is displayed in Fig. 1(a).

The initial pressure profile adopted here takes the form $p_0(r) = (1 - r^2)^5$. In addition, referring to the previous work,[30] three typical rotation profiles with different shear layer positions are adopted, as shown in Fig. 1(b). The rotation equation takes the following form:

$$\omega_{\theta 0} = \frac{1}{r}\frac{\partial \phi_0}{\partial r} = \omega_0[c(1) - c(r)]/[c(1) - c(0)], \quad (5)$$

with $c(r) = \tan^{-1}[(r - r_0)/d_0]$ and $\omega_0 = \omega_{\theta 0}(r = 0)$ being the normalized rotation frequencies on the magnetic axis. The shear locations are set at $r_0 = 0.278$, 0.423 and 0.565, respectively, corresponding to the inner rational surface (rotation 1), $q_{\min}$ (rotation 2), and outer rational surface (rotation 3) positions, respectively. The half width of shear layer d_0 is set as $d_0 = 0.1$ for general cases. The coordinate is selected to rotate with the initial plasma rotation. The radial mesh number is set to $N_r = 1000$. Other typical parameters, if not specially mentioned, are set to $\epsilon = 0.25$, $S_A^{-1} = 5 \times 10^{-7}$, $R^{-1} = 10^{-7}$, $\chi_{\parallel} = 10$, and $\chi_{\perp} = 10^{-7}$.

By adopting the aforementioned initial equilibrium profiles, an explosive burst can occur even where there is no bootstrap current. By including bootstrap current in the simulation, an explosive burst can be brought forward to occur. Figure 2(a) shows the temporal evolution of magnetic island width for different fractions of bootstrap current. The precipitous increase of magnetic island width indicates the occurrence of an explosive burst. This result has also been obtained in a previous work.[29] Note that, in Fig. 2(a), the maximum island width between cases with and without bootstrap current are quite similar. This is not generally the case. In general, the maximum island width for a case with bootstrap current would be larger than for a case without bootstrap current; this is to some extent due to the accelerated release of free energy with the loss of bootstrap current. In this work, due to the small fraction of bootstrap current ($f_b = 0.2$), the maximum island width does not increase significantly in the case with bootstrap current. Wang *et al.*[30] found that differential poloidal rotation, with rotation shear located near the outer rational surface, can effectively prevent the occurrence of an explosive burst. Similar results have also been reproduced in this work, as shown in Fig. 2(b). Without the effect of Coriolis force, the application of differential poloidal rotation will prevent the occurrence of an explosive burst, as the amplitude of rotation exceeds a given threshold. For a simulation including the effect of Coriolis force, the result shown in Fig. 2(c) reveals that this threshold significantly declines. Note that, even including the effect of Coriolis force, the rotation with shear located near the inner rational surface (rotation 1) still does not achieve effective suppression of the explosive burst. As such, the following analysis will focus on the situation under rotations 2 and 3.

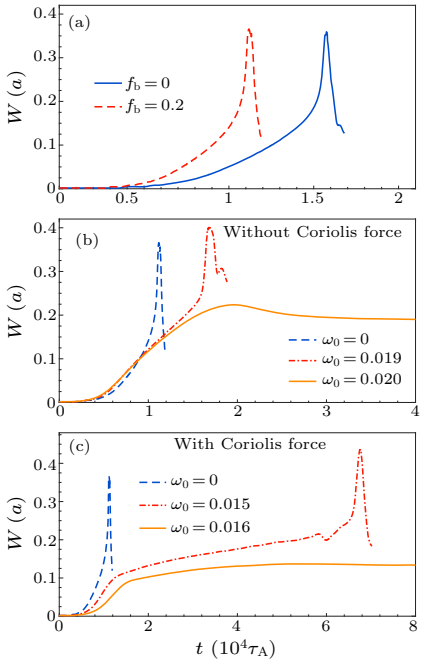

Fig. 2. Temporal evolution of magnetic island in the following cases: (a) without rotation, for different fractions of bootstrap current, (b) with rotation 3, but without Coriolis force, for different amplitudes of rotation, and (c) with both rotation 3 and Coriolis force, for different amplitudes of rotation.

In order to highlight the role of Coriolis force under different conditions, four cases with typical plasma parameters are examined. Here, the modification of initial equilibrium profiles by $m/n = 0/0$ perturbation is included, so that rational surfaces will evolve with time. Figure 3 illustrates the temporal evolution of eight characteristic quantities during the nonlinear process of these cases. Amplitudes of shear rotation adopted in the four cases are just sufficient to suppress the explosive burst. The effect of Coriolis force is neglected only in case 4. By comparing case 1 with case 2, we find that the characteristic quantities in both cases differ only a little, except that the radial positions of $q_{\min}$ and the outer rational surface move in opposite directions. By adopting a different rotation profile (case 2 with rotation 2, and case 3 with rotation 3), the difference is much smaller. From the viewpoint of magnetic island width evolution, in case 2, the island grows faster at first, and then is largely suppressed, leaving a small bump in the curves of Figs. 3(a) and (b). For case 3, however, there is no bump. As long as the shear position of rotation 3 is located at the outer rational surface, the suppression effect is more direct than for rotation 2, located at $q_{\min}$. Nonetheless, in both cases, the amplitudes of shear rotation required to completely suppress an explosive burst show almost no difference.

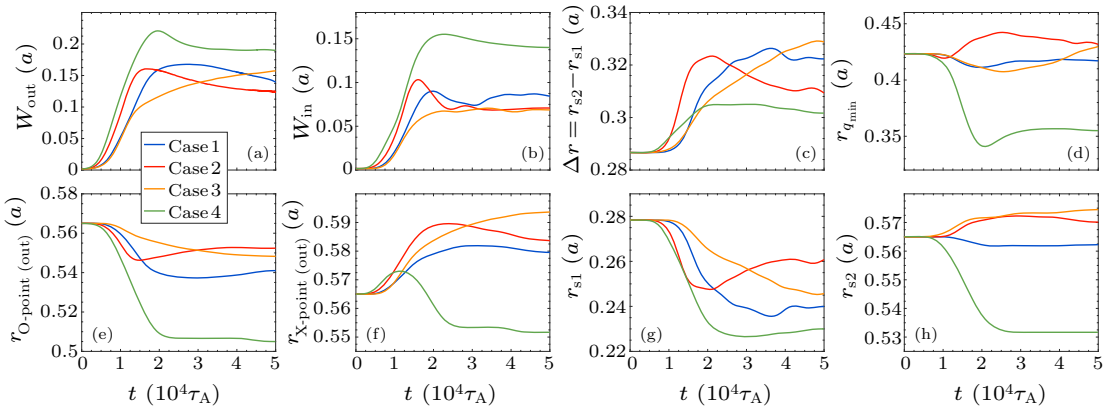

Fig. 3. Temporal evolution of (a) outer magnetic island width, (b) inner magnetic island width, (c) distance between the two $q = 3$ rational surfaces, (d) radial position of q_{min}, (e) outer magnetic island's O-point, (f) outer magnetic island's X-point, (g) inner rational surface, and (h) outer rational surface for cases 1–4. Typical parameters in case 1: $f_b = 0$, $\omega_0 = 0.011$, with rotation 2 and Coriolis force; case 2: $f_b = 0.2$, $\omega_0 = 0.016$, with rotation 2 and Coriolis force; case 3: $f_b = 0.2$, $\omega_0 = 0.016$, with rotation 3 and Coriolis force, and case 4: $f_b = 0.2$, $\omega_0 = 0.020$, with rotation 3 and without Coriolis force.

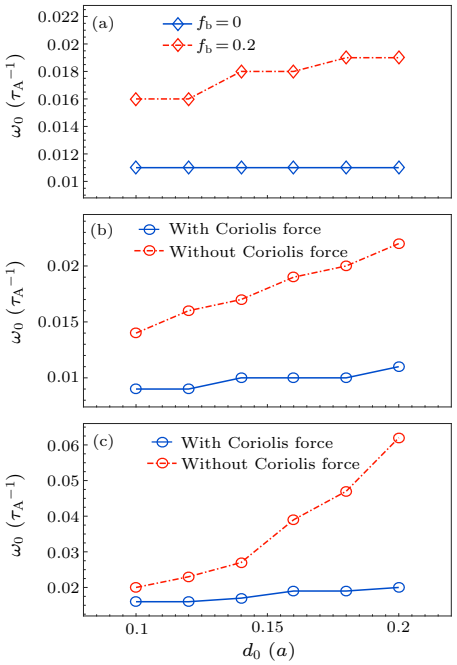

Fig. 4. Amplitude of rotation in order to effectively suppress an explosive burst, versus different shear layer widths of differential rotation under the following parameters: (a) with rotation 2 and Coriolis force, for $f_b = 0$ and $f_b = 0.2$, (b) with rotation 3 and $f_b = 0$, excluding and including Coriolis force, (c) with rotation 3 and $f_b = 0.2$ excluding and including Coriolis force.

The evolution of characteristic quantities in case 4 apparently differs from that observed for the other cases. In case 4, the DTM has the largest saturated magnetic island widths of all the cases under examination, for both inner and outer islands. Saturated magnetic island widths in the other cases hardly differ at all. Due to the fact that, in case 4, both inner and outer rational surfaces are shifting in the direction of the magnetic axis during nonlinear evolution, the separation, Δr_s, between two $q = 3$ rational surfaces does not change much. However, the radial position of q_{min} moves inward to some extent. Both the outer rational surface and the radial position of q_{min} in the other cases hardly change. Generally, the explosive burst is triggered by the strong coupling between inner and outer magnetic islands. The reduction of the coupling effect due to larger rational surface separation during nonlinear evolution is the main reason why, in the case with a Coriolis force effect, smaller shear rotation is required to suppress the explosive burst.

Previous works have reported that shear layer width is another key parameter that may influence the effectiveness of differential poloidal rotations.[30] Therefore, in Fig. 4, we present the amplitude of rotation to effectively suppress an explosive burst, versus different shear layer widths of differential rotation under different conditions. While applying rotation 2, for classical TM ($f_b = 0$), the amplitudes of rotation to effectively suppress an explosive burst show no difference between cases with different shear layer widths. For the case where $f_b = 0.2$, the amplitude increases slightly with increasing shear layer width. The application of rotation 3, and a comparison between cases with and without Coriolis force, are shown in Figs. 4(b) and 4(c). For both $f_b = 0$ and $f_b = 0.2$ conditions, the shear layer width has only a minimal influence on the suppression effectiveness in the case with Coriolis force. However, for the case without Coriolis force effect, the suppression effectiveness drops rapidly with increasing shear layer width. For the case without a Coriolis force effect, the suppressing effect of rotation on the explosive burst is mainly due to the influence on the TM stability index, Δ', of the outer magnetic island, which weakens the coupling effect between the inner and outer islands. Increasing the shear layer width corresponds to reducing the local shear near the outer rational surface, which clearly impairs

suppression effectiveness. In the case with Coriolis force effect, however, a larger rational surface separation can be maintained during the course of temporal evolution, which weakens the coupling effect in a more direct way. Thus, in the case with Coriolis force effect, the suppression effectiveness is less sensitive to shear layer width.

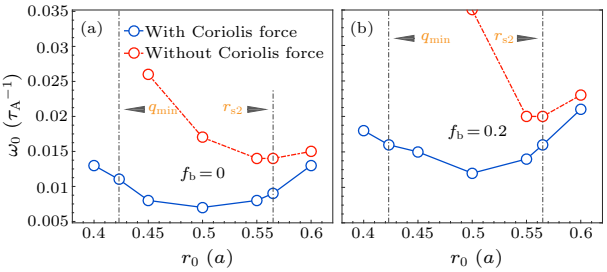

Fig. 5. Amplitude of rotation to effectively suppress an explosive burst, versus different shear layer position of differential rotation under the parameters (a) with $f_b = 0$, excluding and including Coriolis force, (b) with $f_b = 0.2$, excluding and including Coriolis force.

In experiments, it is difficult to accurately control the position of shear rotation, due to operational limitations. It is therefore necessary to explore the effective radial region of shear location. Figure 5 shows the amplitude of rotation to effectively suppress an explosive burst, versus different shear layer positions of differential rotation under different conditions. For the case without a Coriolis force effect, applying shear rotation, with shear located only near the outer rational surface, can effectively suppress an explosive burst. Shifting the shear position towards the magnetic axis can seriously impair suppression effectiveness. For the case with a Coriolis force effect, however, a shear position located between the positions of $q_{\min}$ and the outer rational surface always exhibits superior suppression effectiveness. This means that there is no need to accurately control shear position to ensure its proximity to the outer rational surface in experiments to suppress an explosive burst.

In summary, Coriolis force plays an important role in the suppression of explosive bursts, where differential poloidal rotation is applied. In comparison with cases without Coriolis force, its inclusion evidently reduces the amplitude of rotation required to effectively suppress an explosive burst. Moreover, the effective radial region of rotation shear location is broader in cases with Coriolis force than in those without it. Numerical results show that, with the effect of Coriolis force, the application of rotation with shear located between the positions of $q_{\min}$ and the outer rational surface always results in effective suppression of explosive bursts, reducing the difficulty of controlling them, and thereby preventing plasma disruptions in experiments. The numerical results reported in this work reveal the basic physical feature of the effect of Coriolis force on the suppression of an NTM-triggered explosive burst. However, the initial plasma rotation profile is assumed to be fixed for the sake of simplicity. During nonlinear evolution, the self-generated $m/n = 0/0$ ϕ will modify the initial rotation profile, and thus influence the effect of Coriolis force to some extent. The effect of $m/n = 0/0$ ϕ is not yet clear. It is therefore necessary to investigate this effect further in future research.

Acknowledgement. The authors gratefully acknowledge the provision of computing resources by the Supercomputer Center of Dalian University of Technology.

References

[1] Carrera R, Hazeltine R D and Kotschenreuther M 1986 *Phys. Fluids* **29** 899
[2] Hegna C C and Callen J D 1992 *Phys. Fluids B: Plasma Phys.* **4** 1855
[3] Cai H 2016 *Nucl. Fusion* **56** 126016
[4] Wei L, Wang Z X, Wang J and Yang X 2016 *Nucl. Fusion* **56** 106015
[5] Wang H, Wang Z, Ding Y and Rao B 2015 *Plasma Sci. Technol.* **17** 539
[6] Wang H H, Sun Y W, Shi T H, Zang Q, Liu Y Q, Yang X, Gu S, He K Y, Gu X, Qian J P, Shen B, Luo Z P, Chu N, Jia M N, Sheng Z C, Liu H Q, Gong X Z, and B N W 2018 *Nucl. Fusion* **58** 056024
[7] Fujita T, Ide S, Kamada Y, Suzuki T, Oikawa T, Takeji S, Sakamoto Y, Koide Y, Isayama A, Hatae T, Kubo H, Higashijima S, Naito O, Shirai H and Fukuda T 2001 *Phys. Rev. Lett.* **87** 085001
[8] Crisanti F, Litaudon X, Mailloux J, Mazon D, Barbato E, Baranov Y, Bécoulet A, Bécoulet M, Challis C D, Conway G D, Dux R, Eriksson L G, Esposito B, Frigione D, Hennequin P, Giroud C, Hawkes N, Huysmans G, Imbeaux F, Joffrin E, Lomas P, Lotte P, Maget P, Mantsinen M, Moreau D, Rimini F, Riva M, Sarazin Y, Tresset G, Tuccillo A A and Zastrow K D 2002 *Phys. Rev. Lett.* **88** 145004
[9] Litaudon X, coulet A B, Crisanti F, Wolf R, Baranov Y, Barbato E, coulet M B, Budny R, Castaldo C, Cesario R, Challis C, Conway G, Baar M D, Vries P D, Dux R, Eriksson L, Esposito B, Felton R, Fourment C, Frigione D, Garbet X, Giannella R, Giroud C, Gorini G, Hawkes N, Hellsten T, Hender T, Hennequin P, Hogeweij G, Huysmans G, Imbeaux F, Joffrin E, Lomas P, Lotte P, Maget P, Mailloux J, Mantica P, Mantsinen M, Mazon D, Moreau D, Parail V, Pericoli V, Rachlew E, Riva M, Rimini F, Sarazin Y, Stratton B, Tala T, Tresset G, Tudisco O, Zabeo L, Zastrow K D and contributors J E 2003 *Nucl. Fusion* **43** 565
[10] Greenfield C M, Murakami M, Ferron J R, Wade M R, Luce T C, Petty C C, Menard J E, Petrie T W, Allen S L, Burrell K H, Casper T A, DeBoo J C, Doyle E J, Garofalo A M, Gorelov I A, Groebner R J, Hobirk J, Hyatt A W, Jayakumar R J, Kessel C E, Haye R J L, Jackson G L, Lao L L, Lohr J, Makowski M A, Pinsker R I, Politzer P A, Prater R, Staebler G M, Strait E J, Taylor T S, West W P and Team T D D 2004 *Plasma Phys. Control. Fusion* **46** B213
[11] Pritchett P L, Lee Y C and Drake J F 1980 *Phys. Fluids* **23** 1368
[12] Wang Z X, Wang X G, Dong J Q, Lei Y A, Long Y X, Mou Z Z and Qu W X 2007 *Phys. Rev. Lett.* **99** 185004
[13] Liu T, Yang J F, Hao G Z, Liu Y Q, Wang Z X, Zheng S, Wang A K and He H D 2017 *Plasma Phys. Control. Fusion* **59** 065009

[14] Wang X Q and Wang X G 2015 *Plasma Phys. Control. Fusion* **57** 025019
[15] Wang X Q and Wang X G 2017 *Nucl. Fusion* **57** 016039
[16] Chang Z, Park W, Fredrickson E D, Batha S H, Bell M G, Bell R, Budny R V, Bush C E, Janos A, Levinton F M, McGuire K M, Park H, Sabbagh S A, Schmidt G L, Scott S D, Synakowski E J, Takahashi H, Taylor G and Zarnstorff M C 1996 *Phys. Rev. Lett.* **77** 3553
[17] de Baar M R, Hogeweij G M D, Lopes C N J, Oomens A A M and Schüller F C 1997 *Phys. Rev. Lett.* **78** 4573
[18] Günter S, Schade S, Maraschek M, Pinches S, Strumberger E, Wolf R, Yu Q and Team A U 2000 *Nucl. Fusion* **40** 1541
[19] Takeji S, Tokuda S, Fujita T, Suzuki T, Isayama A, Ide S, Ishii Y, Kamada Y, Koide Y, Matsumoto T, Oikawa T, Ozeki T and Y S 2002 *Nucl. Fusion* **42** 5
[20] Maget P, Huysmans G T A, Garbet X, Ottaviani M, Lütjens H and Luciani J F 2007 *Phys. Plasmas* **14** 052509
[21] Liu T, Wang Z X, Wang J and Wei L 2018 *Nucl. Fusion* **58** 076026
[22] Zhang W, Ma Z, Lu X and Zhang H 2020 *Nucl. Fusion* **60** 126022
[23] Tang W, Wang Z X, Wei L, Wang J and Lu S 2020 *Nucl. Fusion* **60** 026015
[24] Yang S M, Park J K, Na Y S, Wang Z R, Ko W H, In Y, Lee J H, Lee K D and Kim S K 2019 *Phys. Rev. Lett.* **123** 095001
[25] Wang Z, Logan N, Munaretto S, Liu Y, Sun Y, Gu S, Park J K, Hanson J, Hu Q, Strait T, Nazikian R, Kolemen E and Menard J 2019 *Nucl. Fusion* **59** 024001
[26] Zhang W, Ma Z W and Wang S 2017 *Phys. Plasmas* **24** 102510
[27] Ishii Y, Azumi M, Kurita G and Tuda T 2000 *Phys. Plasmas* **7** 4477
[28] Ishii Y, Azumi M and Kishimoto Y 2002 *Phys. Rev. Lett.* **89** 205002
[29] Wang Z X, Wei L and Yu F 2015 *Nucl. Fusion* **55** 043005
[30] Wang J, Wang Z X, Wei L and Liu Y 2017 *Nucl. Fusion* **57** 046007
[31] Wang S and Ma Z W 2015 *Phys. Plasmas* **22** 122504
[32] Ren Z, Liu J, Wang F, Cai H, Wang Z and Shen W 2020 *Plasma Sci. Technol.* **22** 065102
[33] Wei L and Wang Z X 2014 *Nucl. Fusion* **54** 043015
[34] Liu T, Wang J, Wei L and Wang Z X 2020 *Nucl. Fusion* **60** 106009
[35] Yu Q, Günter S, Lackner K, Gude A and Maraschek M 2000 *Nucl. Fusion* **40** 2031
[36] Sato M and Wakatani M 2005 *Nucl. Fusion* **45** 143